

## Article

# Residence Time Distribution of Non-Spherical Particles in a Continuous Rotary Drum

Saeed Mahdavy<sup>1,\*</sup>, Hamid Reza Norouzi<sup>1,\*</sup> , Christian Jordan<sup>2</sup> , Bahram Haddadi<sup>2,\*</sup>  and Michael Harasek<sup>2</sup> 

<sup>1</sup> Center of Engineering and Multiscale Modeling of Fluid Flow (CEMF), Department of Chemical Engineering, Amirkabir University of Technology (Tehran Polytechnic), No. 350, Hafez, Tehran 15875-4413, Iran; saeedmahdavy@aut.ac.ir

<sup>2</sup> Technische Universität Wien, Institute of Chemical, Environmental and Bioscience Engineering, Getreidemarkt 9/166, 1060 Vienna, Austria; christian.jordan@tuwien.ac.at (C.J.); michael.harasek@tuwien.ac.at (M.H.)

\* Correspondence: h.norouzi@aut.ac.ir (H.R.N.); bahram.haddadi.sisakht@tuwien.ac.at (B.H.); Tel.: +98-21-6454-3157 (H.R.N.); +43-1-58801-166252 (B.H.)

**Abstract:** The motion of non-spherical particles with sharp edges, as they are commonly involved in practice, was characterized by residence time distribution (RTD) measurement in a continuous drum. Particles with two sizes, 6 and 10 mm, and two densities, 750 and 2085 kg/m<sup>3</sup>, were used in the experiments. The effects of rotation speed (3–11 rpm), incline angle (2–4°), feed rate, and mixture composition were investigated and compared to the results of other researchers on particles without sharp edges. We also fitted the RTD with an axial dispersion model to obtain a better insight into the flow behavior. MRT of non-spherical particles with sharp edges depends on  $\omega^{-\alpha}$  similar to other shapes, while the value of alpha is higher for particles with sharp edges ( $0.9 < \alpha < 1.24$ ), especially at high incline angles. The MRT depends on incline angle,  $\beta^{-b}$ , where  $b$  varies between 0.81 (at low  $\omega$ ) and 1.34 (at high  $\omega$ ), while it is close to 1 for other shapes. Feed rate has a slight effect on the MRT of particles with sharp edges and the effect of particle size diminishes when rotation speed increases. The MRT linearly increases with volume fraction of light particles in a mixture of light and heavy particles (from pure heavy to pure light particles).

**Keywords:** rotary drum; non-spherical particles; residence time distribution; mean residence time; biomass



**Citation:** Mahdavy, S.; Norouzi, H.R.; Jordan, C.; Haddadi, B.; Harasek, M. Residence Time Distribution of Non-Spherical Particles in a Continuous Rotary Drum. *Processes* **2022**, *10*, 1069. <https://doi.org/10.3390/pr10061069>

Academic Editor: Jianhong Xu

Received: 5 May 2022

Accepted: 25 May 2022

Published: 26 May 2022

**Publisher's Note:** MDPI stays neutral with regard to jurisdictional claims in published maps and institutional affiliations.



**Copyright:** © 2022 by the authors. Licensee MDPI, Basel, Switzerland. This article is an open access article distributed under the terms and conditions of the Creative Commons Attribution (CC BY) license (<https://creativecommons.org/licenses/by/4.0/>).

## 1. Introduction

Rotary drums are used in many industries such as chemical, pharmaceutical, metallurgical, and food processing [1]. They provide good conditions for mixing, drying, coating, granulation, chemical reaction [2], clinkering of cement, regeneration of spent catalyst, and char activation [3]. They can process a wide range of particle sizes and shapes. High construction cost, non-uniform temperature profile, and limited reaction rate between solid and gas are their disadvantages [3].

Rotary drums can be used in batch or continuous processes [4]. In continuous mode, solids are fed into the drum through a feeder. They move forward and mix by a combined action of rotation and gravitation due to inclination of the drum. The time that particles stay in the drum is defined as residence time [5]. Residence time is one of the most important parameters that can be used to evaluate heat and mass transfer conditions and reaction extent in the rotary drum [6]. For instance, if heat transfer derives the drying or reaction of particles, the residence time of particles must be longer than time that is required to accomplish desired drying or reaction [7]. Thus, residence time distribution (RTD) can affect the reaction progress or the pyrolysis performance in the kiln [8].

Plug flow and completely mixed flow are two different ideal models for flow patterns. In reality, solid flow differs from these ideal flow models. Thus, the RTD of particles

deviates from the RTD of plug flow and mixed flow [9]. Many factors affect the RTD, such as the rotation speed of the drum, incline angle, feed rate (as operation variables) [10,11], internal geometry [12], and particle shape [13].

Most of the studies on the RTD measurement in rotary drums are dedicated to spherical particles as reviewed, e.g., by Lu et al. [14], while in industrial application, particles are mostly non-spherical [15,16]. Some other researchers study non-spherical shape in rotary drums via the means of experiments and simulation, such as cylindrical particles (such as broken rice or wood pellet) [10,11,17,18], cuboid particles (such as wood chips or alumina) [5,15,17,19], pharmaceutical tablets [1], ellipsoid particles [20], polyhedral particles [21], and cubic particles [16,18]. In addition, even spherical particles may undergo shape change due to cohesion, breakage, or reaction [7,22]. Non-spherical particles' flow behavior is more complex than spherical particles [23]. For instance, correlations and criteria used for characterizing flow regime for spherical particles may not be used for non-spherical particles [2,20,24].

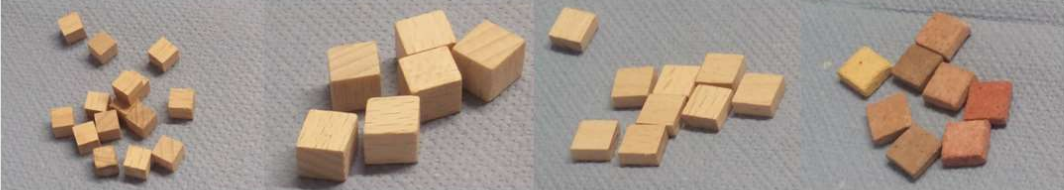
The axial dispersion model (ADM) is used to describe non-ideal solid flow [25]. RTD of solids can be defined as a function of Peclet number. Peclet number includes the combined effect of dispersion coefficient and mean residence time (MRT). Thus, a change in the axial dispersion coefficient or the MRT can lead to a change in the RTD. Variables in the ADM are meaningful and can be compared to other phenomena such as reaction and heat transfer [16,25]. Gao et al. measured RTD of spherical, cylindrical and quadrilobe particles. Their results showed that non-spherical particles have less axial dispersion than spheres [5]. Lu et al. studied axial dispersion coefficient for cubic particles. Their results showed that axial dispersion coefficient depends on rotation speed, acceleration of gravity and volume equivalent diameter [16].

In addition to experiments, discrete element (DEM) simulations answer many unknowns concerning granular flow through accurate modeling of inter-particle interactions. DEM is a robust and mature modeling approach for granular flow. The sub-models of mechanical contact interactions and techniques for representing particle surface are well established for spherical particles, while sub-models and shape representations of non-spherical particles still need improvement [26]. One fundamental step in utilizing DEM for granular flow is to validate simulation results against reliable experimental measurements. Therefore, providing detailed and vast experimental data on the flow behavior of granular flows (especially for non-spherical particles) for DEM-based research is another aim of this research.

Among non-spherical particle with regular and irregular shape, cubic and cuboid particles can be obtained by six cuts, and their dimensions can be easily specified. Thus, we used cubic particles as the model particle for non-spherical particles with sharp edges. Additionally, wooden and ceramic cuboid particles were used in a mixture to find the effect of density variation. This mixture resembles the conditions that the solid flow contains particles with various density (such as wood pyrolysis in rotary kiln with ceramic as a heat carrier [27]). RTD was measured at different rotation speeds, incline angles, feed rates, particle sizes, and volume fraction of wooden particles, and then fitted to the ADM. In all cases, we tried to compare our results with similar results on spherical and non-spherical particles without sharp edge to find the similarities and the differences between their flow behavior. All the experimental results on RTD were also provided as Supplementary Data to be used by other researchers who are aiming to validate their DEM simulation results.

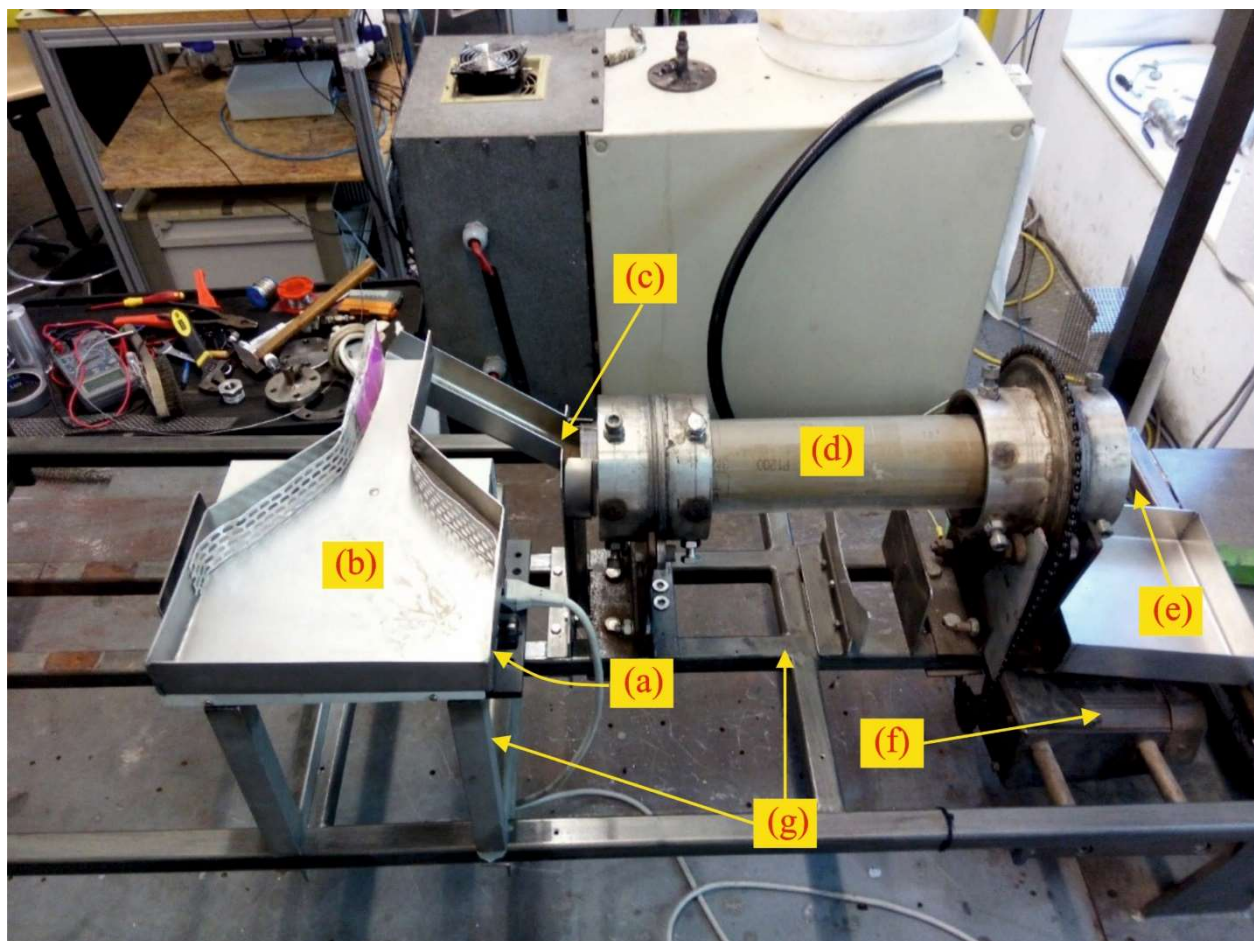
## 2. Material and Procedure

Figure 1 shows the shape and properties of particles that we used in this study. The dimensions of cubic wooden particles were  $6 \times 6 \times 6 \text{ mm}^3$  and  $10 \times 10 \times 10 \text{ mm}^3$ . We also tested the variation in the density with cuboid ceramic (heavy) and wooden (light) particles whose dimensions were  $4 \times 10 \times 10 \text{ mm}^3$ . The density variation is important, since, in reality, ceramic particles can be used as heat carriers in the system [27].

				
<b>Material</b>	<b>Wood</b>	<b>Wood</b>	<b>Wood</b>	<b>Ceramic</b>
<b>Shape</b>	<b>Cubic</b>	<b>Cubic</b>	<b>Cuboid</b>	<b>Cuboid</b>
<b>Size (mm<sup>3</sup>)</b>	6 × 6 × 6	10 × 10 × 10	4 × 10 × 10	4 × 10 × 10
<b>Density</b> ( $\frac{kg}{m^3}$ )	660	660	750	2085

**Figure 1.** Particle shapes and their properties.

All experiments were performed in a rotary drum with length 50.0 cm, inside diameter 8.4 cm, and outside diameter 9.0 cm and at room temperature. The drum was made of plexiglas with very smooth surface. This smooth surface could not resemble the actual roughness of the rotary kilns in practice. Therefore, a thin sandpaper P1200 was affixed to the inside surface of the drum to achieve the desirable roughness in the surface. Figure 2 shows the experimental setup including parts that were used in this research.



**Figure 2.** Rotary drum setup and its parts: (a) vibrator (b) particle feeder (c) inlet of particles into drum (d) rotary drum (e) outlet of drum (f) motor (g) setup support.

A three-phase AC motor (400 V) was used with a frequency inverter for rotation speed control. The feeder was vibrated using a Retsch DR 100 vibrator (Retsch, Hann, Germany) to achieve the desired flow rate of particles. The incline angle of the support of the kiln was changed by a jack. Table 1 lists experimental conditions. Rotation speed varied between 3 rpm to 11 rpm; incline angle, between 2° to 4°; and feed rate, between 0.67 cm<sup>3</sup>/s and 1.08 cm<sup>3</sup>/s for cubic particles. Cuboid particles (wood and ceramic mixture) were used to determine the effect of density at 7 rpm and 2°, whereas the volume fraction of wood was varied in the mixture of wood and ceramic particles.

We used colored particles as the tracers. When rotary drum operation reached steady state condition, these colored tracers were fed into the drum. A Samsung HMX-F90 camera, located near the outlet of drum, recorded the particles' movement and their exit moments. Entrance and exit times of each tracer give us the residence time. Recorded videos were processed by Kdenlive 19.12.3. Each experiment was repeated three times. Figure 3 demonstrates cross view of drum at different rotation speed, incline angle and feed rate for 6 mm and 10 mm cubes. Tracers are particles with dark color.

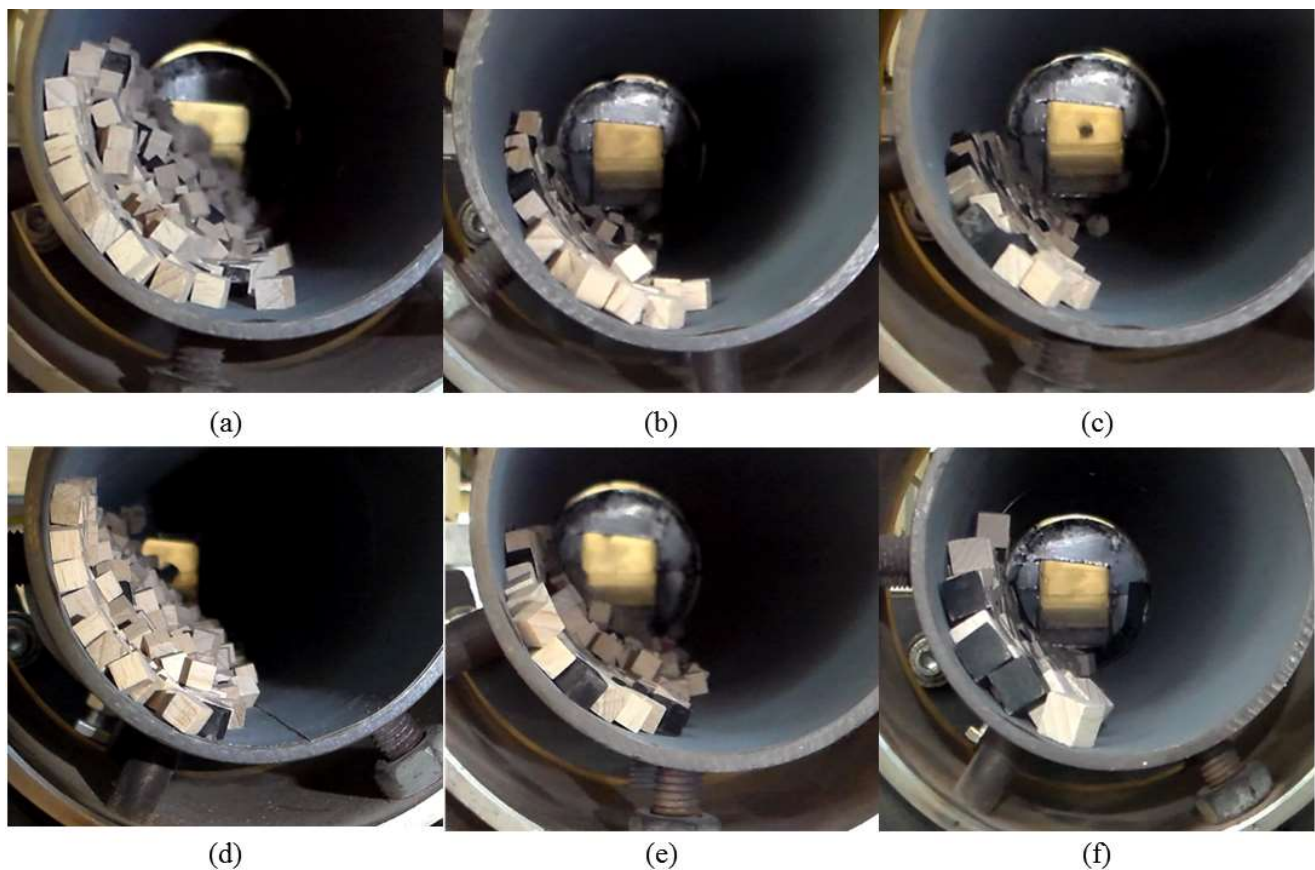


**Figure 3.** Cross view of drum at (a) 3 rpm, 3°, and 1.08 cm<sup>3</sup>/s for 6 mm cubes (b) 7 rpm, 3°, and 1.08 cm<sup>3</sup>/s for 6 mm cubes (c) 11 rpm, 3°, and 1.08 cm<sup>3</sup>/s for 6 mm cubes (d) 3 rpm, 2°, and 1.08 cm<sup>3</sup>/s for 6 mm cubes (e) 3 rpm, 3°, and 0.67 cm<sup>3</sup>/s for 6 mm cubes (f) 3 rpm, 3°, and 1.08 cm<sup>3</sup>/s for 10 mm cubes (black particles are tracer).

Table 1. Run conditions.

Run. No	Rotation Speed (rpm)	Incline Angle (°)	Feed Rate (cm <sup>3</sup> /s)	Size (mm <sup>3</sup> )	Shape	Number of Tracer (-)	Wood Volume Fraction (-)
1	3						
2	5						
3	7	2					
4	9						
5	11						
6	3						
7	5						
8	7	3					
9	9						
10	11		1.08				
11	3			6 × 6 × 6		50	
12	5						
13	7	4					
14	9						
15	11						
16	5	2.5					
17	11						
18	5	3.5					
19	11						
20	3				cube		1
21	7	3	0.67				
22	11						
23	3						
24	5						
25	7	2					
26	9						
27	11						
28	3						
29	5						
30	7	3					
31	9						
32	11		1.08	10 × 10 × 10		30	
33	3						
34	5						
35	7	4					
36	9						
37	11						
38	5	2.5					
39	11						
40	5	3.5					
41	11						
42			0.28			50	0
43			0.31				0.25
44	7	2	0.34	10 × 10 × 4	cuboid	60	0.5
45			0.37				0.75
46			0.40			50	1

### 3. Residence Time Distribution (RTD)

The system reaches a steady-states condition when the numbers of entering and exiting particles are the same. After that, tracers are entered into the drum. Figure 4 shows the method used for introducing the tracers. We used 30–60 tracer particles in each experiment.

Sixty tracers were used in the run numbers 42–46 (effect of volume fraction of the wood). For example, when the volume fraction of wood is 0.25, the number of tracers for wood is 25% of all tracers, hence 15 black tracers are wood, and 45 red tracers are ceramic (see Figure 4b).

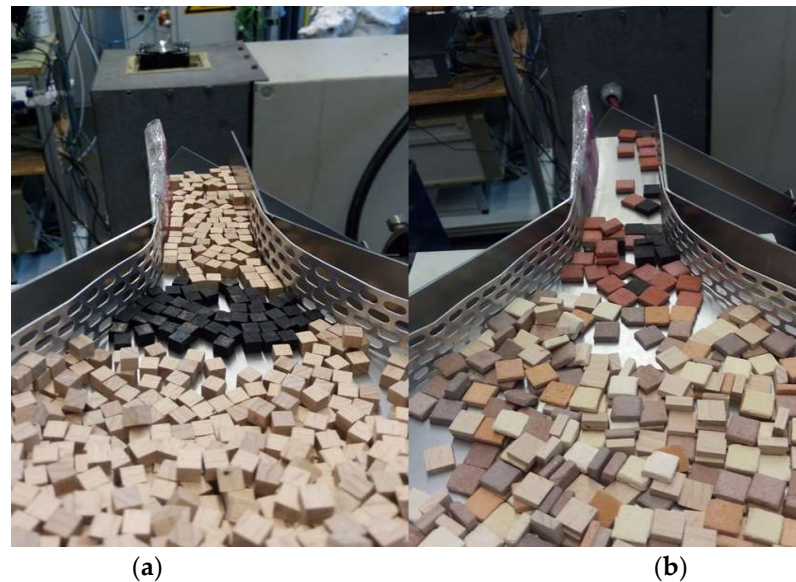


**Figure 4.** Introduction of tracers into the feeder for single component and two components, (a) black tracer for 6 mm cubes (b) black wood tracer and red ceramic tracer for wood-ceramic mixture ( $x_{\text{wood}} = 0.25$ ).

Entrance and exit moments of tracer in the drum were recorded by camera. Residence time of a tracer is the difference between these two moments. The cumulative distribution function,  $F(t)$ , demonstrates the fraction of tracers that have left the drum until  $t$ .  $F(t)$  is computed by [28]:

$$F(t) = \frac{N(t)}{N_0} \quad (1)$$

where  $N(t)$  is number of tracer particles that left the drum until  $t$ , and  $N_0$  is total number of tracer particles. The mean residence time (MRT) is obtained by:

$$\text{MRT} = \frac{1}{N_0} \sum_{i=1}^n t_i \quad (2)$$

where  $t_i$  is residence time of tracer.

#### 4. The Axial Dispersion Model (ADM)

A one-dimensional axial dispersion model (ADM) was used for fitting experimental data. This model describes convective-dispersive transport of particles at unsteady state condition without reaction [28,29].

$$\frac{L}{u_z} \frac{\partial C(z,t)}{\partial t} = \frac{1}{Pe} \frac{\partial^2 C(z,t)}{\partial z^2} - \frac{\partial C(z,t)}{\partial z} \quad (3)$$

where  $C(z,t)$  shows dimensionless tracer concentration,  $z$  is dimensionless length ( $z = l/L$ ),  $l$  is position of tracer in the axial direction,  $t$  is time,  $u_z$  is the mean axial velocity,  $L$  is the drum length, and  $Pe$  is the Peclet number.

$Pe$  number indicates the ratio of convective mass transport to dispersive mass transport. If the  $Pe$  number is high, the convective mass transport is dominant; while if  $Pe$  number is

low, the dispersion is dominant. A narrow time distribution is obtained when  $Pe$  number is high, while a wide distribution is obtained when  $Pe$  number is low.

$$Pe = \frac{u_z \cdot L}{D_{ax}} \quad (4)$$

where  $D_{ax}$  is axial dispersion coefficient, as a measure for erratic movement [10].

All dispersion is assumed to happen in the drum; which means that the tracer concentration gradient begins from the drum inlet by dispersion and convection (Equation (5)) and ends at the drum outlet (Equation (6)) [28,29].

$$C_{in} = C_{(0+,t)} - \frac{1}{Pe} \frac{\partial C}{\partial z} \Big|_{z=0+} \quad (5)$$

$$\frac{\partial C}{\partial z} \Big|_{z=1} = 0 \quad (6)$$

ADM equation with above boundary conditions is solved numerically [28,29], though the analytical solution can be found for  $Pe > 50$  [30]. An implicit finite difference method was used to solve ADM according to the above boundary conditions. Solution of ADM gives the tracer concentration at all positions and times.  $C(z = 1, t)$  shows the concentration of tracer at the drum outlet that depends on  $Pe$ . Time distribution changes due to changes in  $Pe$ . Average absolute square error (AASE) was defined (Equation (7)), to find the best fitted curve of ADM on experimental data. The nearest curve is obtained based on the minimum value of AASE. MRT is obtained from the experiment based on Equation (2). Consequently, the axial dispersion coefficient is calculated by Equation (4). `fminbnd` function is used in MATLAB R2018b to minimize AASE.

$$\text{Average Absolute Square Error (AASE)} = \frac{\sum_{i=1}^n (F_{\text{experiment}} - F_{\text{ADM}})^2}{N_0} \quad (7)$$

## 5. Result and Discussion

Figure 5 shows the cumulative residence time distributions obtained from experiments and fitted with the ADM. The cumulative residence time distribution,  $F(t)$ , shows the fraction of tracers that has left the drum. It includes RTD results of three rotation speeds (3, 7, and 11 rpm), three incline angles (2, 3 and 4°), and two feed rates (0.67 and 1.08 cm<sup>3</sup>/s) for 6 mm cubes. The ADM fitted curves can describe one-dimensional flow behavior in the drum very well. The difference between the first and the last tracer residence time for 3 rpm (Figure 5a) is approximately 550 s. For the two other cases (7 rpm and 11 rpm), these differences are approximately 300 s and 80 s; therefore, when rotation speed increases, tracers leave the drum faster, and RTD becomes narrower. Figure 5d compares cumulative residence time distribution at three different rotation speed. A narrower distribution is obtained due to higher rotation speed. Other researchers have also shown that narrower RTD are obtained when rotation speed increases [5,7,10,24,31–33]. Figure 5e shows the effect of the incline angle on the RTD. When the incline angle increases, the residence time of particles decreases and RTD becomes narrower. Previous studies similarly showed that RTD becomes narrower when incline angle increases [7,10,24,33]. Figure 5f compares the RTD results of 6 mm at two different flow rates. According to Figure 5f, an increase in the feed causes a slight shift to higher values of RTD. The shapes of RTD curves at two flow rates are similar. Njeng et al. [33] showed that feed rate had a slight effect on RTD curves for cuboid particles.

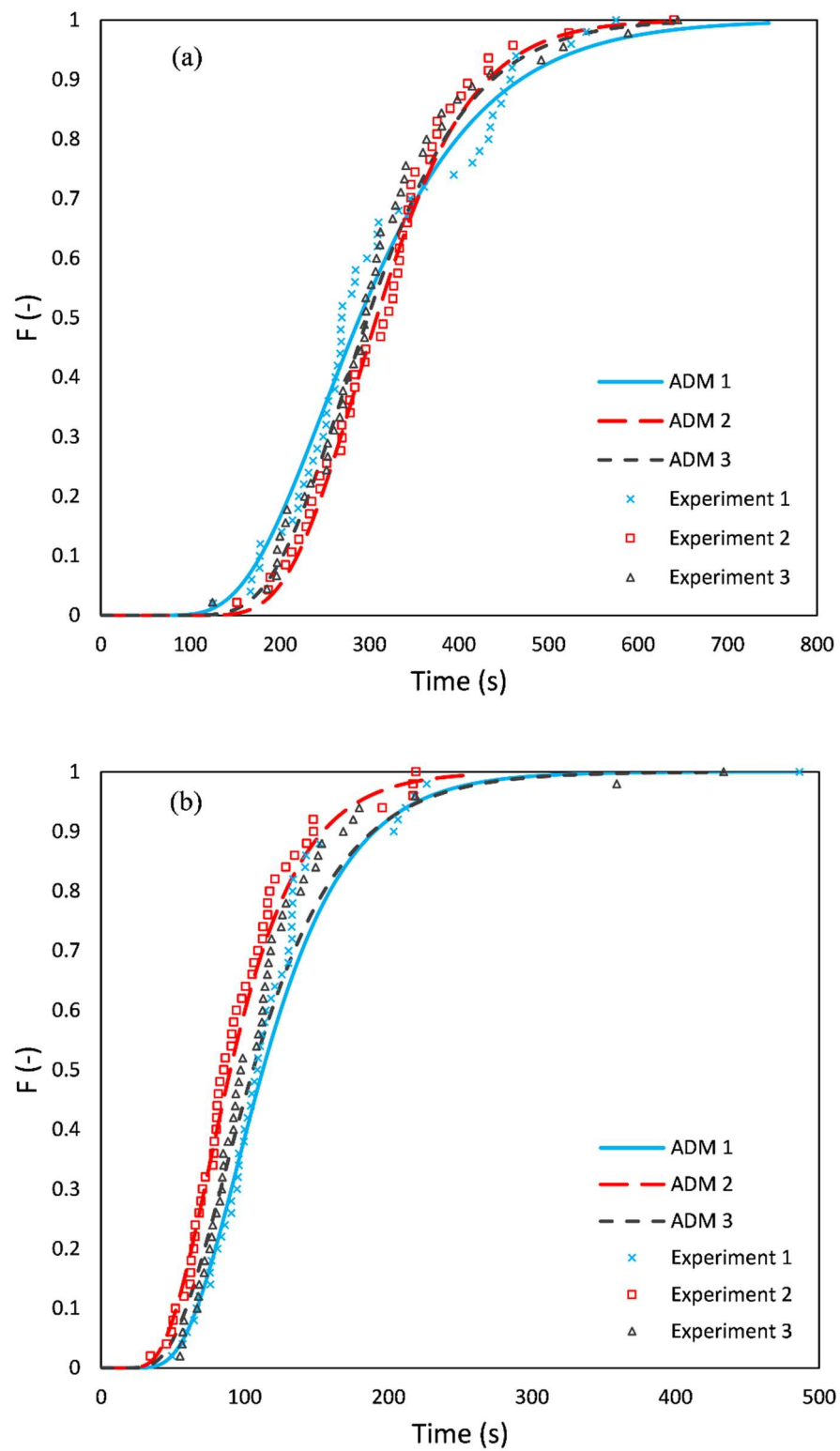


Figure 5. Cont.

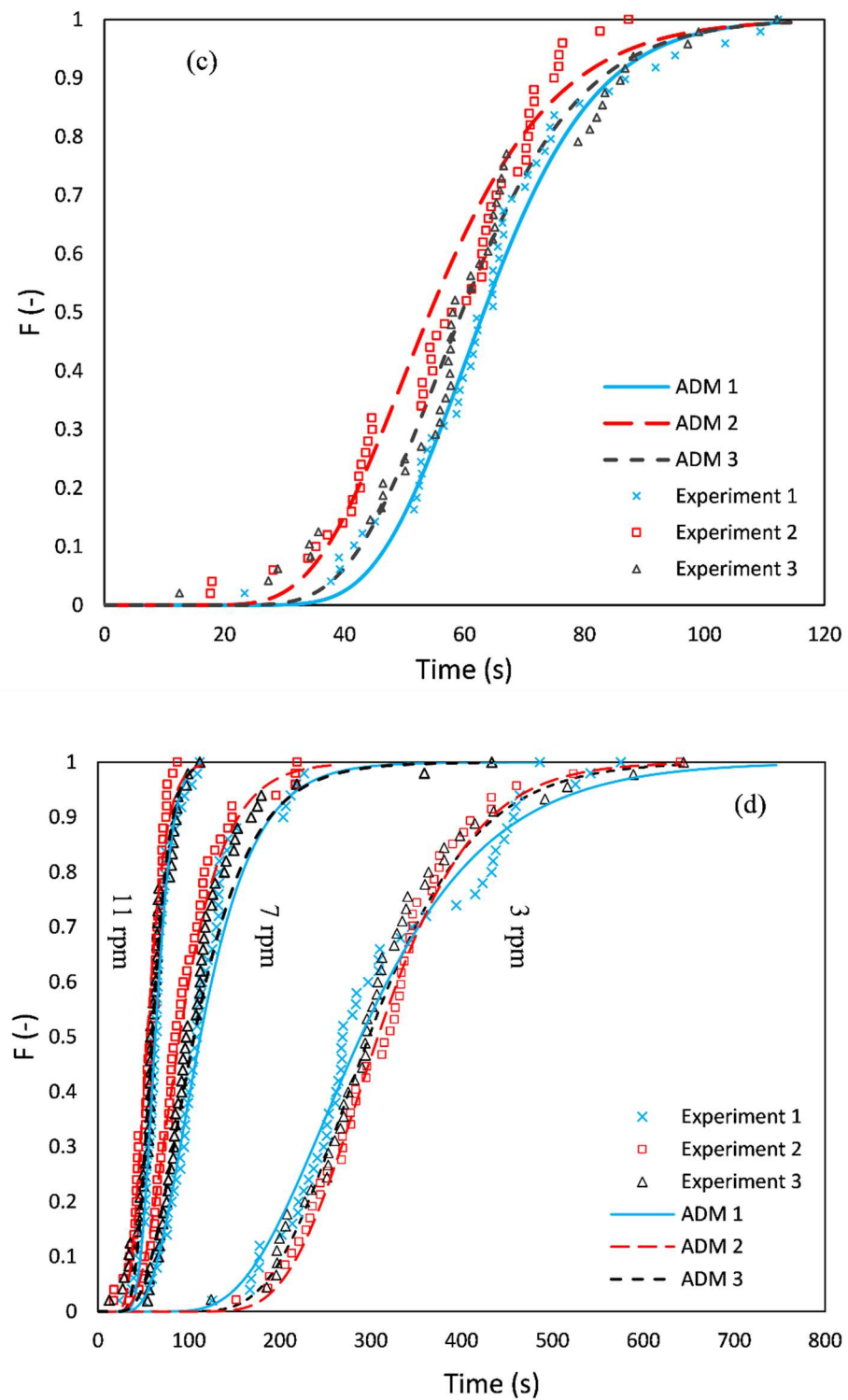
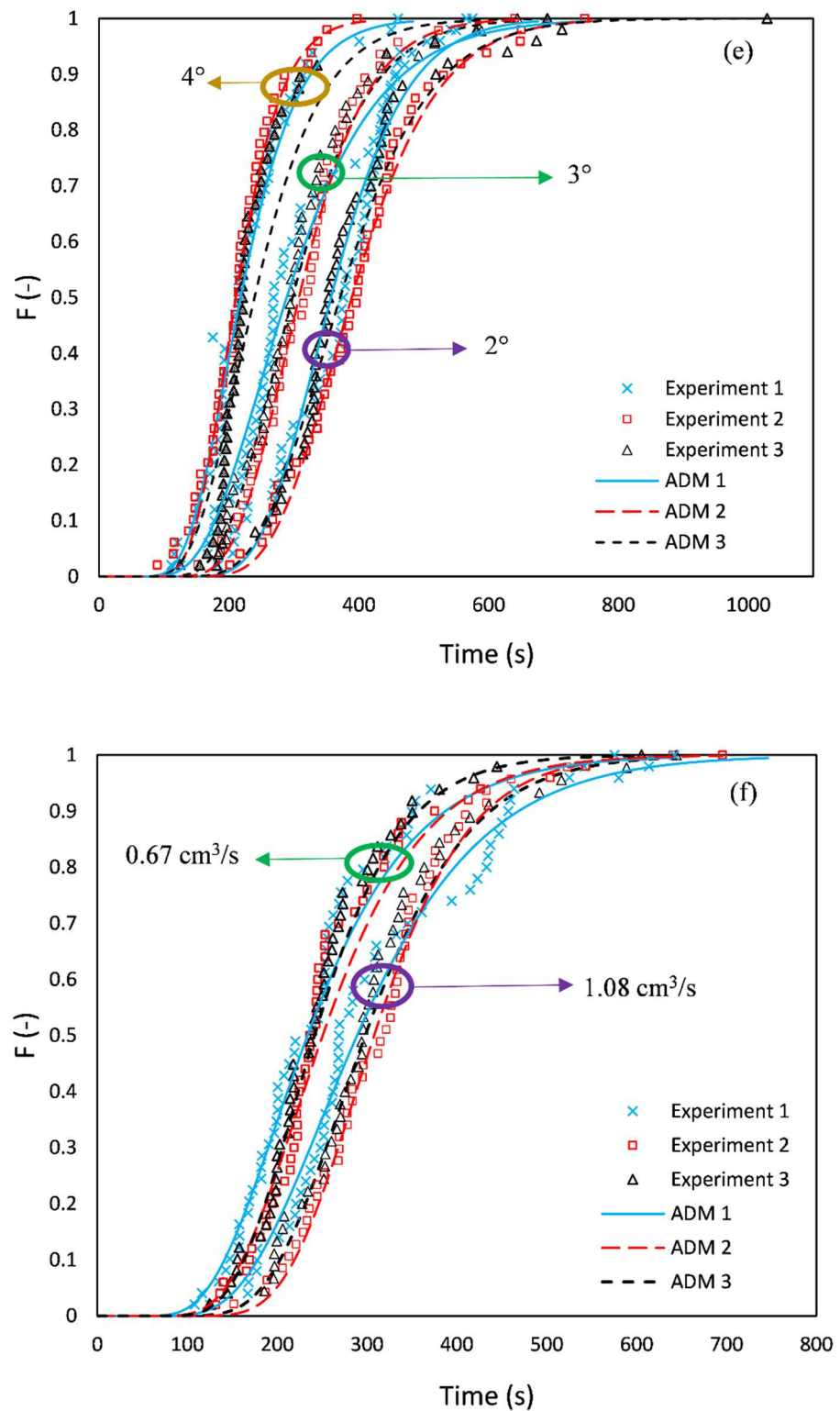


Figure 5. Cont.



**Figure 5.** Cumulative distribution as a function of outlet time in experiments and fitted with ADM (a) 3 rpm,  $3^\circ$ , and  $1.08 \text{ cm}^3/\text{s}$  for 6 mm cubes; (b) 7 rpm,  $3^\circ$ , and  $1.08 \text{ cm}^3/\text{s}$  for 6 mm cubes; (c) 11 rpm,  $3^\circ$ , and  $1.08 \text{ cm}^3/\text{s}$  for 6 mm cubes; (d) 3–11 rpm,  $3^\circ$  and  $1.08 \text{ cm}^3/\text{s}$  for 6 mm cubes; (e) 3 rpm,  $2\text{--}4^\circ$  and  $1.08 \text{ cm}^3/\text{s}$  for 6 mm cubes; (f) 3 rpm,  $3^\circ$  and  $0.67$  and  $1.08 \text{ cm}^3/\text{s}$  for 6 mm cubes. (Each experiment repeated 3 times and ADM model was fitted on the three sets of data.)

Table 2 shows the results of Figure 5a–c. MRTs of each row are obtained from the experiment based on Equation (2).  $Pe$ ,  $AASE$ , and  $D_{ax}$  are obtained from ADM. An increase

in the rotation speed led to a decrease in the MRT. The MRT value changes from 313 s to 61 s when the rotation speed is increased from 3 to 11 rpm. Axial dispersion coefficient increases when rotation speed changes from 3 rpm to 7 rpm; however, it decreases when rotation speed changes from 7 rpm to 11 rpm.

**Table 2.** Results of experiment and ADM at 3° and 1.08 cm<sup>3</sup>/s for 6 mm cubes. (Each experiment was repeated 3 times and ADM model was fitted on the three sets of data.)

Rotation Speed		MRT [s]		Pe. No [-]	AASE [-]	D <sub>ax</sub> [cm <sup>2</sup> /s]
3 rpm	Experiment 1	310.0	ADM 1	12.4	2.1 × 10 <sup>-3</sup>	0.651
	Experiment 2	318.8	ADM 2	26.0	9.0 × 10 <sup>-4</sup>	0.290
	Experiment 3	311.5	ADM 3	20.7	1.5 × 10 <sup>-3</sup>	0.386
	Average	313.4		19.7	1.5 × 10 <sup>-3</sup>	0.442
	Standard deviation	3.9		5.6		0.153
7 rpm	Experiment 1	122.2	ADM 1	10.2	3.6 × 10 <sup>-3</sup>	1.997
	Experiment 2	98.1	ADM 2	9.5	1.1 × 10 <sup>-3</sup>	2.664
	Experiment 3	116.9	ADM 3	8.0	3.4 × 10 <sup>-3</sup>	2.660
	Average	112.4		9.2	2.7 × 10 <sup>-3</sup>	2.440
	Standard deviation	10.4		0.9		0.313
11 rpm	Experiment 1	64.7	ADM 1	38.5	1.5 × 10 <sup>-3</sup>	1.002
	Experiment 2	56.5	ADM 2	22.2	4.1 × 10 <sup>-3</sup>	1.987
	Experiment 3	61.4	ADM 3	29.7	2.5 × 10 <sup>-3</sup>	1.368
	Average	60.9		30.1	2.7 × 10 <sup>-3</sup>	1.452
	Standard deviation	3.4		6.7		0.407

In the following sections, we present the effects of rotation speed, incline angle, feed rate, particle size and density on the MRT and the axial dispersion coefficient. All the RTD experimental data and ADM analysis results can be found in the Supplementary Data that accompanies this article. The data are stored in the spreadsheet (Microsoft Excel) format. The data can be used for validation DEM simulations for non-spherical particles.

### 5.1. Effect of Rotation Speed

Figure 6a shows the effect of rotation speed on MRT for 6 mm cubes in which rotation speed changes from 3 rpm to 11 rpm at three different incline angles while feed rate is fixed at 1.08 cm<sup>3</sup>/s. The error bars also show the interval change in mean with the confidence level of 95%. An exponential model was used to find the relationship between rotation speed and MRT. Regressed equations are presented in the figure. On average, particles remain shorter in the drum when rotation speed increases. At low rotation speeds (3–5 rpm), the rotation speed has a greater effect on MRT than high rotation speeds. MRT decreases when incline angle increases. The figure indicates an overall 69 % decrease in the MRT when the rotation speed changes from 3 rpm to 11 rpm at 2° incline angle. This change in MRT is more notable for higher incline angle values.

When the incline angle increases, the magnitude of exponents of rotation speed ( $\omega$ ) in the regressed equations in the figure also increases ( $|-0.899| < |-1.227| < |-1.242|$ ), which shows that rotation speed has a more pronounced effect on the MRT at higher incline angles. Previous studies showed that  $MRT \propto \omega^{-1}$ ,  $MRT \propto \omega^{-0.98}$ , and  $MRT \propto \omega^{-0.88}$  for spherical particles [7,34,35]. Njeng et al. [33] established a relationship for spherical and non-spherical particles (broken rice and beech chips) which shows  $MRT \propto \omega^{-0.884}$ . Gao et al. [5] showed that the effect of rotation speed on the MRT of spherical particles is not same as non-spherical particles (cylindrical and cuboid). Our results show that the magnitude of the exponent for cubic particles with sharp edges is higher than that for spherical and non-spherical particles without sharp edge (see Table 3 to compare the operating conditions in this research with others).

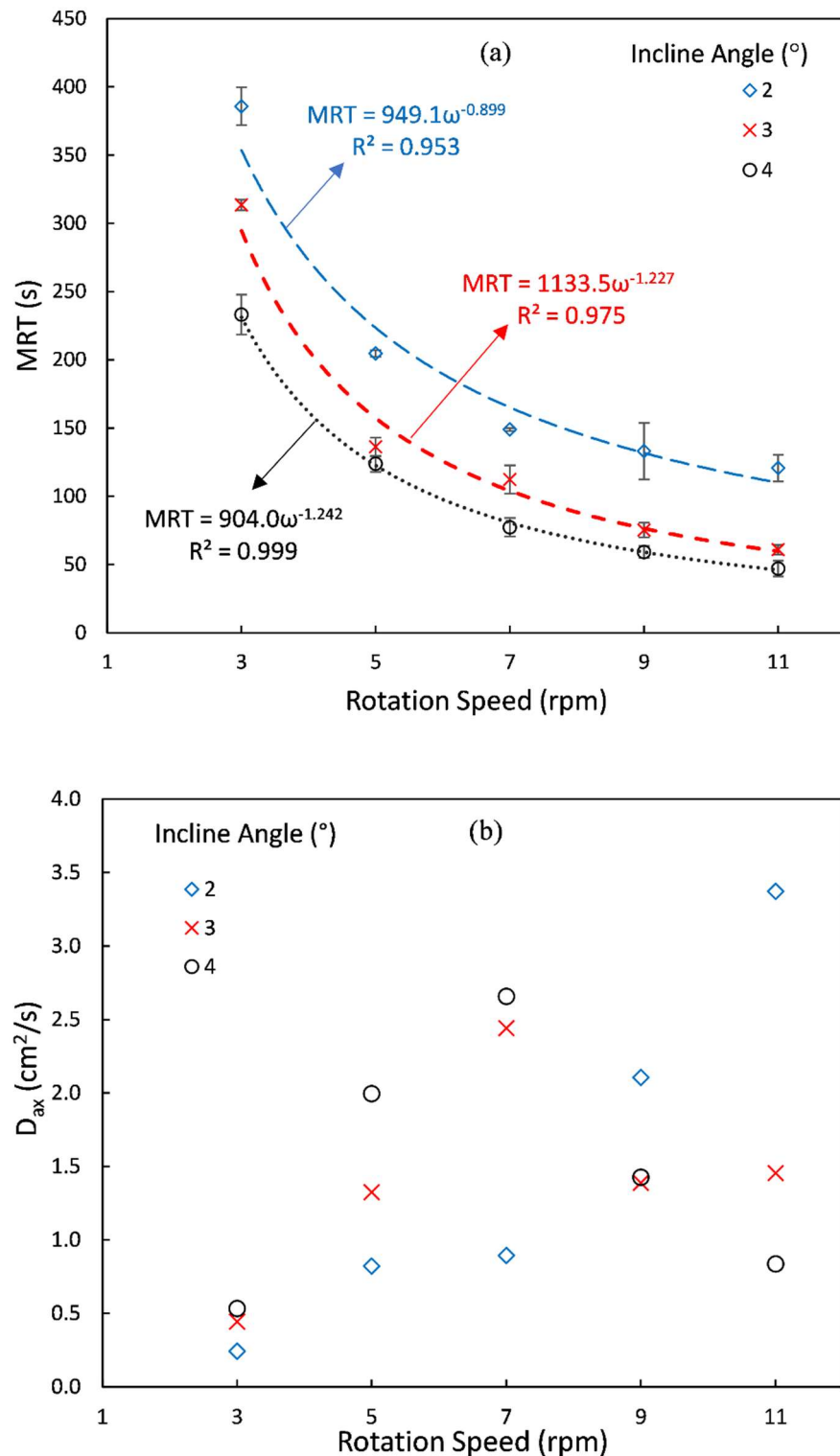


**Figure 6.** Effect of rotation speed on (a) MRT (b) axial dispersion coefficient at 1.08 cm<sup>3</sup>/s for 6 mm cube.

Figure 6b shows the effect of rotation speed on the axial dispersion coefficient at three incline angles. At 2° of incline angle, the axial dispersion coefficient increases with rotation speed. This behavior can also be seen for other incline angles (3° and 4°) up to 7 rpm, while after 7 rpm, the axial dispersion coefficient decreases. When the rotation speed increases, particles rise to a higher height on the drum wall, detach and avalanche from that height. This means that avalanching particles on the surface have more chance of having random

motions on the surface (contrary to the particles in layers below the surface). It should be noted that the axial dispersion coefficient shows random displacement of particles [10]. Generally, other studies showed that axial dispersion coefficient increases with rotation speed for cohesive powder and catalyst [7,31], spherical particles [10,11,34], cylindrical particles [10,10,36], cuboid particles [33] and cubic particles [16].

**Table 3.** Comparison between operating conditions, drum geometry and particle shape in the literature with this research.

	L (cm)	D (cm)	Shape	dp * (mm)	$\omega$ (rpm)	$\beta$ ( $^{\circ}$ )	dp/D (-)	L/D (-)	$\omega^2 \cdot R/g$ (-)
Sai et al. [34]	590	14.7	sphere	1.1	1–3	0.78–1.37	0.0075	40.14	$8.2 \times 10^{-5}$ – $7.4 \times 10^{-4}$
Sherritt et al. [37]	90	20	sphere	3	5–25	0	0.015	4.5	$2.8 \times 10^{-3}$ – $7.0 \times 10^{-2}$
Third et al. [38]	15.2	10	sphere	1–3	2.5–30	0	0.01–0.03	1.52	$6.9 \times 10^{-5}$ – $3.3 \times 10^{-1}$
Lu et al. [16]	15.2	10	cube	1.692–3.384 (2–4)	2.5–30	0	0.02–0.04	1.52	$6.9 \times 10^{-5}$ – $4.9 \times 10^{-1}$
Njeng et al. [33]	420	21	cuboid	$10 \times 4.5 \times 2$ (5.56)	2–6	1–3	0.026	20	$4.7 \times 10^{-4}$ – $4.2 \times 10^{-3}$
Chen et al. [31]	323.23 and 600.46	15.24 and 33.02	sphere	0.070	1–13	1.1–3	0.00046 & 0.00021	18.18 & 21.21	$8.5 \times 10^{-5}$ – $3.1 \times 10^{-2}$
This research	50	8.4	Cube and cuboid	6–10 (7.44–12.41)	3–11	2–4	0.089–0.148	5.95	$4.2 \times 10^{-4}$ – $5.7 \times 10^{-3}$

\* Diameter of equivalent sphere was reported in the parenthesis for non-spherical particles.

Reviewing the captured movies in the experiments revealed that a change in flow behavior occurs at 9 rpm when the incline angle is  $3^{\circ}$  and  $4^{\circ}$  and the bed flow behavior is similar to slumping regime. Sherritt et al. [37] indicated that for slumping regime, the axial dispersion coefficient decreased when rotation speed increased. Our results beyond 7 rpm at  $3^{\circ}$  and  $4^{\circ}$  incline angle show a similar effect. Thus, increasing rotation speed has an inverse effect on axial dispersion coefficient.

### 5.2. Effect of Incline Angle

Figure 7 illustrates the effect of incline angle on the MRT and the axial dispersion coefficient. Figure 7a shows the effect of incline angle on the MRT at two different rotation speeds and feed rate  $1.08 \text{ cm}^3/\text{s}$  for 6 mm cubes. In addition, the power law functions were regressed on the data and equations are presented in the figure. MRT decreases as the incline angle increases. MRT does not change too much between  $3^{\circ}$  to  $4^{\circ}$ , while this effect is considerable from  $2^{\circ}$  to  $3^{\circ}$ . An increase in the rotation speed at each incline angle causes a shift of MRT to a lower value (almost 80 s in each case). The effect of incline angle on the MRT is similar to the effect of rotation speed, so we can write  $\text{MRT} \propto \beta^{-a}$  (where  $\beta$  indicates incline angle). The relations  $\text{MRT} \propto \beta^{-1.054}$  and  $\text{MRT} \propto \beta^{-1.02}$  can be found for spherical particles [7,34,35], while Njeng et al. [33] showed that  $\text{MRT} \propto \beta^{-0.928}$  for spherical and non-spherical particles. Our results show a wider span of exponent for non-spherical particles with sharp edges. This indicates that the incline angle has a stronger dependency on the MRT than it does on spherical and non-spherical particles without sharp edges.

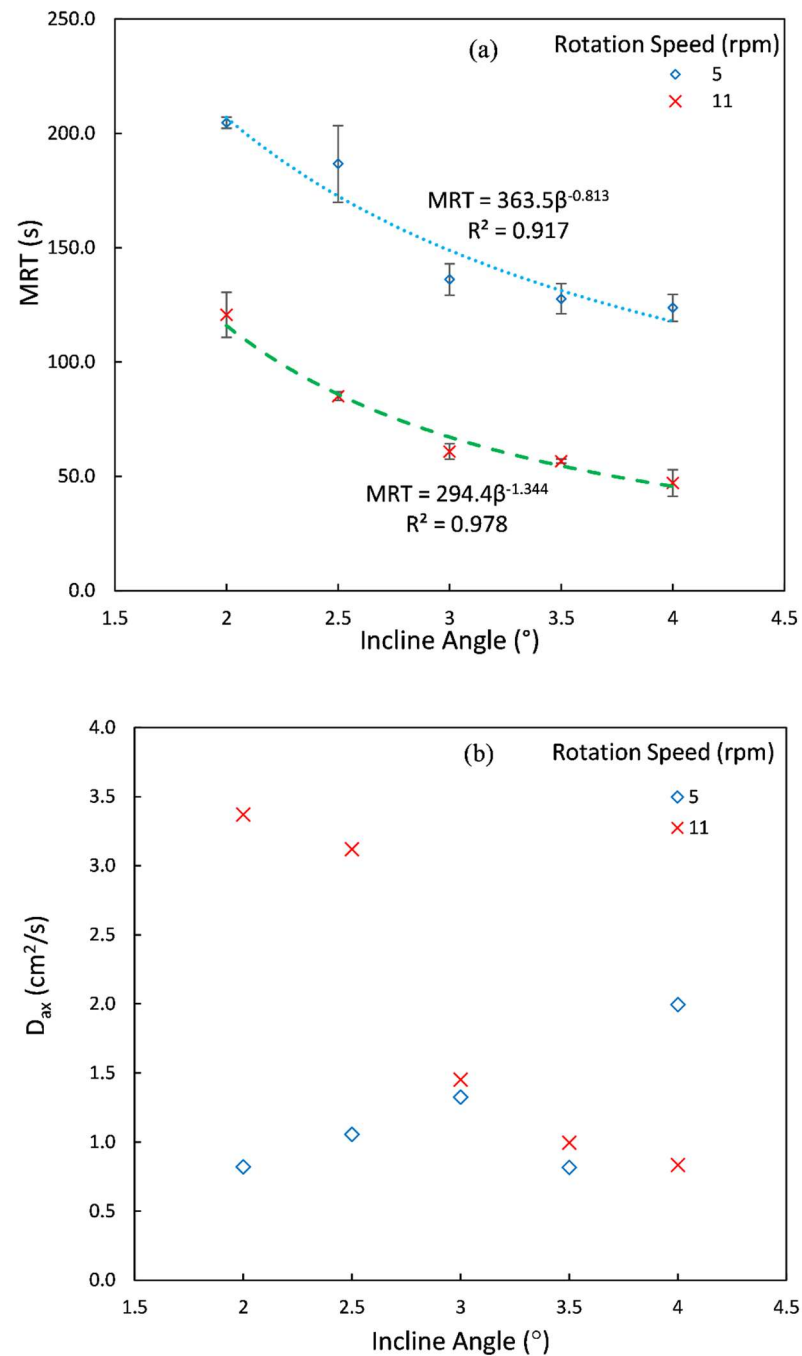


**Figure 7.** Effect of incline angle on (a) MRT (b) axial dispersion coefficient at 1.08 cm<sup>3</sup>/s for a 6 mm cube.

In Figure 7b, when incline angle increases, axial dispersion coefficient increases (except at 3.5°) at 5 rpm. The standard deviation of axial dispersion coefficient at 3°, 3.5° and 4° are, respectively, equal to 0.058, 0.376 and 0.803 cm<sup>2</sup>/s, which clearly shows that the reduction in the average value at 3.5° is not statistically significant. The axial dispersion coefficient decreases as the incline angle increases at 11 rpm. When the rotation speed is high, the number of particles in the drum is low and only one or, at most, two layers of particles are formed, which means that there is directed motion of particles rather than random motion of particles during avalanching. Consequently, the axial dispersion coefficient decreases.

### 5.3. Effect of Feed Rate

The effects of feed rate on the MRT and the axial dispersion coefficient are shown in Figure 8 at 3° incline angle for 6 mm cubes. When the feed rate decreases, the number of particles and formed layers decrease, and hence, residence time decreases. Figure 3a,e illustrate that a decrease in feed rate leads to a decrease in the fill level in the drum. On average, particles remain for a shorter time in the drum when the feed rate decreases. This fact is more considerable at low rotation speeds. When rotation speed increases from 3 rpm to 7 rpm, the flowability of particles in the drum enhances and, hence, the difference between the MRTs of different feed rate decreases. An 11 rpm feed rate does not have a significant effect on the MRT. Other studies also confirm slight effect of feed rate on the MRT. For instance, Gao et al. [5] observed that the MRT was weakly influenced by feed rate for sphere, cylinder or cuboid. Similar results were observed for cuboid particles by Njeng et al. [33] and for cylindrical particles by Sudah et al. [36]. It is noteworthy that changing feed rate can slightly change the MRT, which was reported in previous research [5,7,11,33–35,39,40]. Our results have good qualitative agreement with other studies [5,7,11,33–35,39,40].

Figure 8b shows that the feed rate does not have a pronounced effect on the axial dispersion coefficient. At 3 rpm and 11 rpm, the values of axial dispersion coefficient are close together, whereas at 7 rpm they are far from together. In other studies, usually, when the feed rate increased, the axial dispersion coefficient decreased [10,33]. This shows that the randomness of particle movement decreases when the feed rate decreases. However, there were some cases in which feed rate had a direct effect on axial dispersion coefficient. Sudah et al. [36] observed that for cylindrical particles, the axial dispersion coefficient decreased from 0.1 cm<sup>2</sup>/s to 0.034 m<sup>2</sup>/s when the feed rate increased from 0.46 cm<sup>3</sup>/s to 1.83 cm<sup>3</sup>/s; and then it gradually increased to 0.042 cm<sup>2</sup>/s when the feed rate further increased to 4.34 cm<sup>3</sup>/s. Gao et al. [5] showed that the axial dispersion coefficient of cuboid particles did not change as a function of feed rate, but feed rate had a small effect on the axial dispersion coefficient of cylindrical particles, and had a more noticeable effect on the axial dispersion coefficient of spherical particles. Our results at 7 rpm do not follow these trends from other literature.

### 5.4. Effect of Particle Size

Figure 9 shows the effect of particle size on the MRT and the axial dispersion coefficient. To understand the effect of size, 6 mm and 10 mm cubes at 3° were compared at the same volumetric flow rate (1.08 cm<sup>3</sup>/s). At these conditions, we observed a lower number of large particles in the drum (see Figure 3a,f). When size increases, the number of particles decreases and then particle–particle and particle–wall interactions decrease. Then, on average, the MRT decreases with an increase in the size. Other studies also confirm these results [41,42]. When rotation speed increases, the flowability of particles in the drum increases, and then the difference between MRT for 6 mm cubes and 10 mm decreases. Nafsun et al. [43] showed a similar effect of particle size on the thermal mixing time for changes in rotational speed (thermal mixing time is directly proportional to the MRT). They discovered that at a high rotation speed effect of particle size diminishes, but at low rotation speeds, particle size had an significant effect on the thermal mixing time [43].

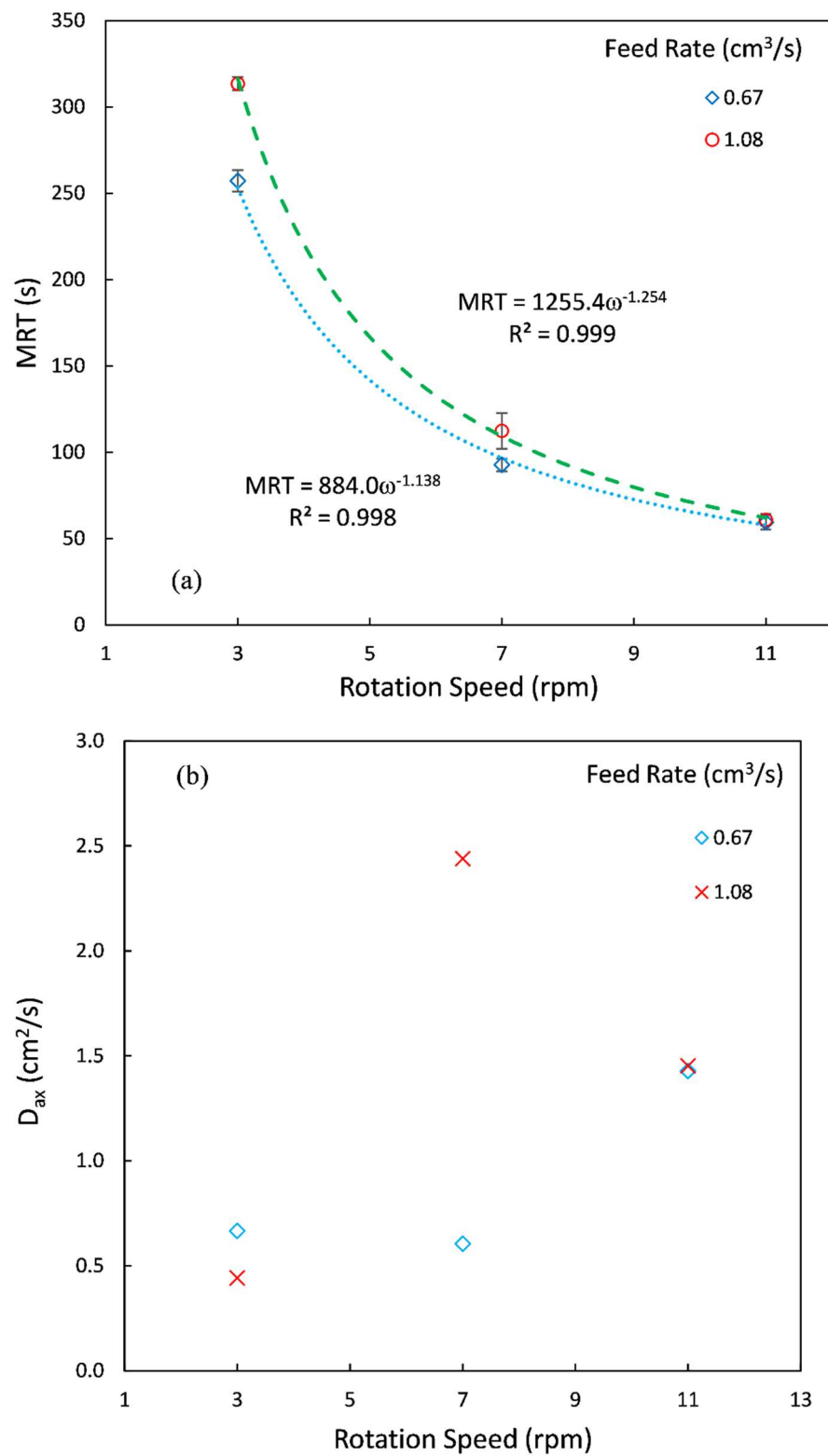


**Figure 8.** Effect of feed rate on (a) MRT (b) axial dispersion coefficient at 3° for 6 mm cube.

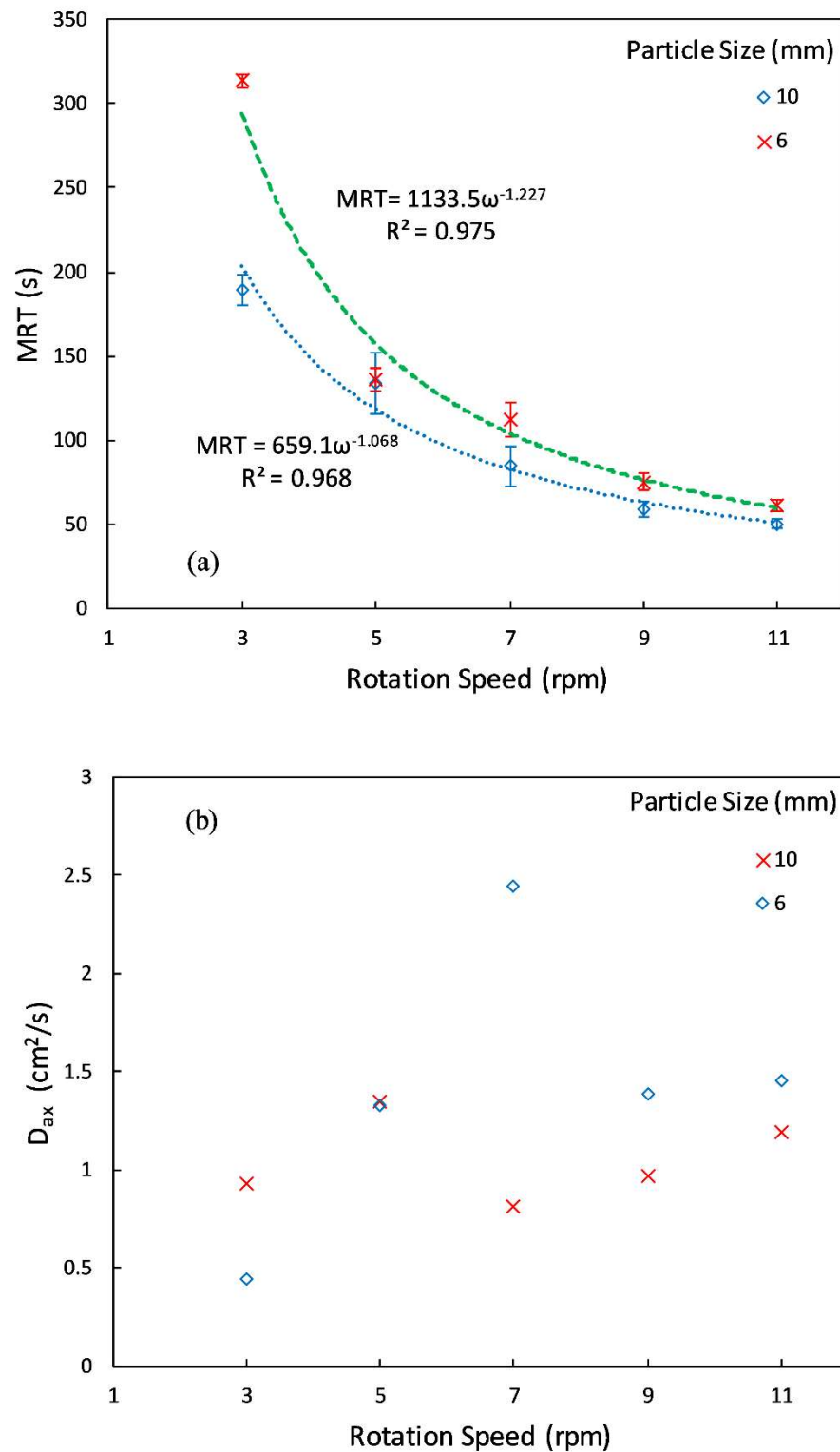


**Figure 9.** Effect of particle size on (a) MRT (b) axial dispersion coefficient at 3° and 0.72 cm<sup>3</sup>/s for 6 mm and 10 mm cube.

The axial dispersion coefficient for larger particles is lower than that for smaller particles (see Figure 9b). This shows that smaller particles are dispersed better. Rotation speed does not significantly affect the axial dispersion coefficient for 10 mm cubes, while rotation speed has a notable effect on the axial dispersion coefficient for 6 mm cubes (see Figure 9b). Bensmann et al. [42] showed that when particle size is increased from 0.55 mm

to 1.5 mm, the axial dispersion coefficient is increased from 0.019 cm<sup>2</sup>/s to 0.240 cm<sup>2</sup>/s, and then decreased to 0.035 cm<sup>2</sup>/s.

### 5.5. Effect of Mixture Composition in the Feed

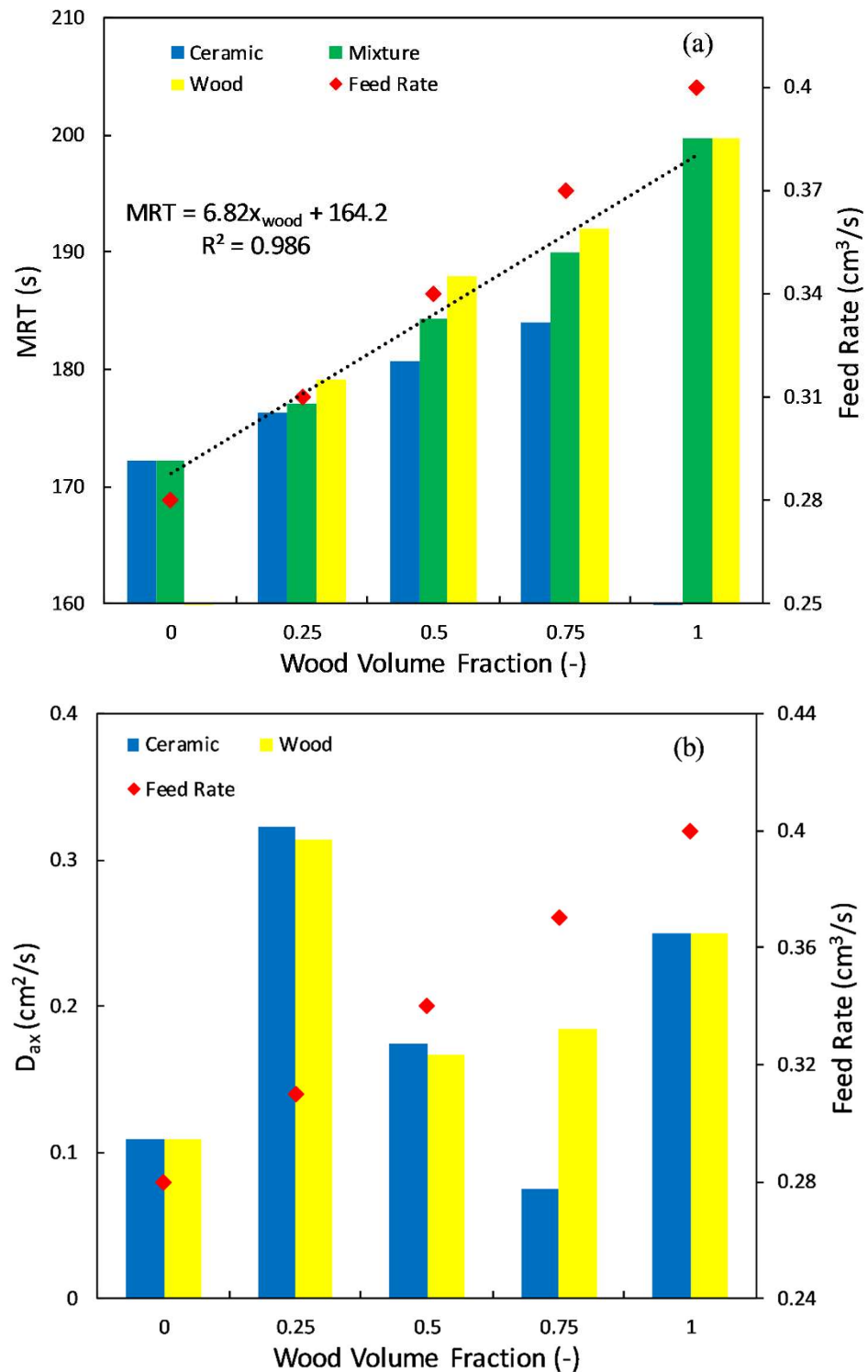
Ceramic and wooden particles of the same size (10 × 10 × 4 mm<sup>3</sup>) were entered into the drum to study the effect of volume fraction of heavy and light particles. Rotation speed and incline angle were fixed at 7 rpm, and 2°, while wood and ceramic volume fractions were changed. The number of tracers of each kind (wooden and ceramic) was proportional to the volume fraction of each particle in the mixture. We could not fix the feed rate at the various volume fractions due to the changes in the density. Therefore, in this series of experiments, feeder vibration was kept constant and we let the feed rate change with volume fraction. The feed rate increased when the wood volume fraction increased in the experiments. For example, for pure ceramic (wood volume fraction = 0) the feed rate was 0.28 cm<sup>3</sup>/s, while for pure wood, it was 0.40 cm<sup>3</sup>/s. In Figure 8a, we showed that the feed rate does not significantly change the MRT of particles in the drum. Based on this observation, we can still draw some conclusions about the pure effect of wood volume fraction on the MRT (without considering the fact that feed rate changes with wood volume fraction).

Figure 10a shows the effect of wood volume fraction in the feed on the MRT (the ceramic volume fraction is 1-wood volume fraction). Since we could distinguish between wood and ceramic particles in the outlet, we calculated separate MRTs for wooden and ceramic particles. Then, the mixture MRT is calculated by Equation (8).

Wood particles stay for a longer time in the drum than ceramic particles. This is mainly related to the higher weight of the wood particles relative to the ceramic particles. Reviewing the captured movies in the experiment, we observed that the mixture sticks to the wall of the drum and rise with the wall. At a certain point, they detach from the wall and avalanche down. During avalanching, ceramic particles travel a longer axial distance (the drum is inclined). This process is repeated a number of times until the particles exit the drum. Thus, ceramic particles stay a shorter time in the drum. The MRT of the mixture is also shown in this figure. We provided a linear regression for the MRT of the mixture as a function of wood volume fraction. It clearly shows that the MRT of the wood and ceramic mixture (particles with different densities) can be linearly interpolated by using the MRTs of pure particles. The regressed line of the MRT of the mixture in Figure 10a shows that the MRT of mixture is a linear function of wood volume fraction:

$$\text{MRT}_{\text{mixture}} = \sum_{i=1}^2 x_i \times \text{MRT}_i \quad (8)$$

Figure 10b shows the effect of wood volume fraction on the axial dispersion coefficient. When wood volume fraction changes, the axial dispersion coefficient does not change notably. Therefore, a change in the wood volume fraction in the mixture does not have a significant effect on the axial dispersion coefficient in this range of operating conditions. We could not find a clear trend for axial dispersion coefficient; however, the maximum of axial dispersion values was observed at the wood volume fraction of 0.25.



**Figure 10.** Effect of volume fraction of light (wood) and heavy (ceramic) cuboid particles on (a) the MRT (b) the axial dispersion coefficient at 7 rpm and 2°.

## 6. Conclusions

Understanding the motion pattern of non-spherical particles in a continuous rotary drum is of great importance for design and scaleup of pyrolysis processes, food manufacturing processes, etc. The motion pattern of spherical particles is characterized by RTD measurements that reflect the cumulative effect of motion of individual particles in the drum. RTD was measured in a continuous rotary drum with the length 50.0 cm and internal

diameter 8.4 cm, using colored particles as tracers. Non-spherical particles with sharp edges were selected in the experiments, since in practice we are facing this class of shapes rather than spherical or non-spherical particles without sharp edges.

Particles with two sizes, 6 and 10 mm, and two densities, 750 and 2085 kg/m<sup>3</sup>, were used in experiments. We included the particles with two densities in our experiments to resemble the condition in which wooden particles (as pyrolysis media) are processed along with ceramic materials (as heat carrier media). In the experiments, rotation speeds varied between 3 and to 11 rpm; incline angle, between 2 and 4°; and feed rate, between 0.28 cm<sup>3</sup>/s to 1.08 cm<sup>3</sup>/s. The effect of mixture composition (a mixture of low- and high-density particles) on the RTD was also investigated. We also fitted the RTD data with the axial dispersion model to obtain a better insight on the flow behavior of particles in the drum. The results were compared with those from similar studies on spherical and non-spherical particles without sharp edges to better understand the similarities and differences between the two (particles with sharp edges and without sharp edges). All the experimental results on RTD are also provided as supplementary data to be used by other researchers who are aiming to validate their DEM simulation results.

Our results showed that the MRT of non-spherical particles with sharp edges depends on  $\omega^{-\alpha}$  similar to other shapes (spherical and non-spherical particles without sharp edge), but the exponent is higher in our experiments ( $0.9 < \alpha < 1.24$ ), especially at high incline angles. At rotation speeds between 3 and 7 rpm, the axial dispersion coefficient increased with rotation speed, while this trend was not observed with further increase in the rotation speed due to change in the flow regime in the drum. The MRT also depends on incline angle  $MRT \propto \beta^{-b}$ , where  $b$  varies between 0.81 (at low rotation speed) to 1.34 (high rotation speed). However, the exponent  $b$  is closer to 1 for other particles with other shapes, suggesting the more pronounced role of incline angle on the particle motion for particles with sharp edges. The axial dispersion coefficient increases with incline angle at 5 rpm and it decreases with increasing the incline angle at 11 rpm. When feed rate increases, fill level increases, and consequently the MRT increases, especially at low rotation speed. Feed rate does not affect the axial dispersion coefficient in our experiments. Smaller particle has higher MRT than bigger particle. We could show that the value of  $\alpha$  in the relation  $MRT \propto \omega^{-\alpha}$  is higher for smaller particles and the difference between MRT of large and small particles diminishes as the rotation speed increases. Rotation speed has a significant effect on the axial dispersion coefficient of 6 mm cubes, while rotation speed has a small effect on the axial dispersion coefficient of 10 mm cubes. Wooden particles (low density) have higher MRT than ceramic particles (high density). For a mixture of wooden and ceramic particles, the MRT linearly increases with volume fraction of wooden particles in a mixture. The MRT of mixture scales with the MRT of pure wooden and ceramic particles, with volume fraction as the scaling factor.

**Supplementary Materials:** The following supporting information can be downloaded at: <https://www.mdpi.com/article/10.3390/pr10061069/s1>, Supplementary data includes a Microsoft excel file named data.xlsx. The first sheet of this file lists experimental conditions table (similar to Table 1 of the article). That sheet has hyperlinks to the corresponding experimental data. The rest of the sheets contain the residence time of tracers and cumulative distribution of residence time (F) in experiments and fitted curves obtained from the ADM. In addition, the calculate MRT,  $Pe$  and  $D_{ax}$  of particles are available in each sheet.

**Author Contributions:** Conceptualization, H.R.N., B.H. and M.H.; methodology, S.M. and B.H.; software, S.M.; validation, S.M. and B.H.; formal analysis, S.M.; investigation, S.M.; resources, C.J.; data curation, S.M., B.H. and C.J.; writing—original draft preparation, S.M.; writing—review and editing, H.R.N., C.J. and B.H.; visualization, S.M.; supervision, H.R.N., B.H. and C.J.; project administration, M.H.; funding acquisition, M.H. All authors have read and agreed to the published version of the manuscript.

**Funding:** Open Access Funding by TU Wien.

**Institutional Review Board Statement:** Not applicable.

**Informed Consent Statement:** Not applicable.

**Data Availability Statement:** Not applicable.

**Acknowledgments:** The authors would like to thank Mario Pichler, Florian Wesenauer and Franz Winter who helped us in this research.

**Conflicts of Interest:** The authors declare no conflict of interest.

## Nomenclature

### symbols

$C(t)$	Dimensionless concentration of tracers at the drum outlet as a function of time, (-)
$C_0$	Initial dimensionless concentration, (-)
$d$	Particle diameter, (m)
$D_{ax}$	Axial dispersion coefficient, (cm <sup>2</sup> /s)
$F(t)$	Cumulative distribution as a function of time, (-)
$l$	Position of tracer in the axis direction of drum, (-)
$L$	Drum length, (m)
$N_0$	Total number of tracer particles, (-)
$N(t)$	Number of tracer particles leave the drum until $t$ as a function of time, (-)
$Pe$	Peclet number, (-)
$t$	Time, (s)
$u_z$	Linear velocity, (m/s)
$x$	Volumetric fraction in the mixture, (-)
$z$	Dimensionless length ( $\frac{l}{L}$ ), (-)
$\beta$	Incline angle of drum, (°)
$\omega$	Rotation speed of drum, (rpm; 1/min)

### abbreviation

ADM	Axial dispersion model
MRT	Mean residence time, (s)
RTD	Residence time distribution

## References

- Dubé, O.; Alizadeh, E.; Chaouki, J.; Bertrand, F. Dynamics of Non-Spherical Particles in a Rotating Drum. *Chem. Eng. Sci.* **2013**, *101*, 486–502. [[CrossRef](#)]
- Norouzi, H.R.; Zarghami, R.; Mostoufi, N. Insights into the Granular Flow in Rotating Drums. *Chem. Eng. Res. Des.* **2015**, *102*, 12–25. [[CrossRef](#)]
- Kunii, D.; Chisaki, T. *Rotary Reactor Engineering*; Elsevier: Amsterdam, The Netherlands, 2007; ISBN 0080553338.
- Boateng, A.A. *Rotary Kilns: Transport Phenomena and Transport Processes*; Butterworth-Heinemann: Oxford, UK, 2015; ISBN 0128038535.
- Gao, Y.; Glasser, B.J.; Ierapetritou, M.G.; Cuitino, A.; Muzzio, F.J.; Beeckman, J.W.; Fassbender, N.A.; Borghard, W.G. Measurement of Residence Time Distribution in a Rotary Calciner. *AIChE J.* **2013**, *59*, 4068–4076. [[CrossRef](#)]
- Hamawand, I.; Yusaf, T. Particles Motion in a Cascading Rotary Drum Dryer. *Can. J. Chem. Eng.* **2014**, *92*, 648–662. [[CrossRef](#)]
- Paredes, I.J.; Yohannes, B.; Emady, H.N.; Muzzio, F.J.; Maglio, A.; Borghard, W.G.; Glasser, B.J.; Cuitiño, A.M. Measurement of the Residence Time Distribution of a Cohesive Powder in a Flighted Rotary Kiln. *Chem. Eng. Sci.* **2018**, *191*, 56–66. [[CrossRef](#)]
- Pichler, M.; Haddadi, B.; Jordan, C.; Norouzi, H.; Harasek, M. Influence of Particle Residence Time Distribution on the Biomass Pyrolysis in a Rotary Kiln. *J. Anal. Appl. Pyrolysis* **2021**, *158*, 105171. [[CrossRef](#)]
- Levenspiel, O. *Chemical Reaction Engineering*; John Wiley & Sons: Hoboken, NJ, USA, 1999; ISBN 047125424X.
- Bongo Njeng, A.S.; Vitu, S.; Clause, M.; Dirion, J.L.; Debaq, M. Effect of Lifter Shape and Operating Parameters on the Flow of Materials in a Pilot Rotary Kiln: Part I. Experimental RTD and Axial Dispersion Study. *Powder Technol.* **2015**, *269*, 554–565. [[CrossRef](#)]
- Bongo Njeng, A.S.; Vitu, S.; Clause, M.; Dirion, J.L.; Debaq, M. Effect of Lifter Shape and Operating Parameters on the Flow of Materials in a Pilot Rotary Kiln: Part II. Experimental Hold-up and Mean Residence Time Modeling. *Powder Technol.* **2015**, *269*, 566–576. [[CrossRef](#)]
- Priessen, J.; Kreutzer, T.; Irgat, G.; Behrens, M.; Schultz, H.J. Solid Flow in Rotary Drums with Sectional Internals: An Experimental Investigation. *Chem. Eng. Technol.* **2021**, *44*, 300–309. [[CrossRef](#)]
- Santos, D.A.; Barrozo, M.A.S.; Duarte, C.R.; Weigler, F.; Mellmann, J. Investigation of Particle Dynamics in a Rotary Drum by Means of Experiments and Numerical Simulations Using DEM. *Adv. Powder Technol.* **2016**, *27*, 692–703. [[CrossRef](#)]

14. Lu, G.; Third, J.R.; Müller, C.R. Discrete Element Models for Non-Spherical Particle Systems: From Theoretical Developments to Applications. *Chem. Eng. Sci.* **2015**, *127*, 425–465. [[CrossRef](#)]
15. Gu, C.; Fan, J.; Pan, D.; Yao, S.; Dai, L.; Guan, L.; Wu, K.; Yuan, Z. Effect of Baffle Structure on the Dynamic Transportation Behavior of S-Liked Biomass Fuels in a Rotating Drum. *Energy Sci. Eng.* **2020**, *9*, 743–756. [[CrossRef](#)]
16. Lu, G.; Third, J.R.; Müller, C.R. The Parameters Governing the Coefficient of Dispersion of Cubes in Rotating Cylinders. *Granul. Matter* **2017**, *19*, 12. [[CrossRef](#)]
17. Fantozzi, F.; Colantoni, S.; Bartocci, P.; Desideri, U. Rotary Kiln Slow Pyrolysis for Syngas and Char Production from Biomass and Waste—Part I: Working Envelope of the Reactor. *J. Eng. Gas Turbines Power* **2007**, *129*, 901–907. [[CrossRef](#)]
18. Hlosta, J.; Jezerská, L.; Rozbroj, J.; Žurovec, D.; Nečas, J.; Zegzulka, J. DEM Investigation of the Influence of Particulate Properties and Operating Conditions on the Mixing Process in Rotary Drums: Part 2-Process Validation and Experimental Study. *Processes* **2020**, *8*, 184. [[CrossRef](#)]
19. Maione, R.; Kiesgen De Richter, S.; Mauviel, G.; Wild, G. DEM Investigation of Granular Flow and Binary Mixture Segregation in a Rotating Tumbler: Influence of Particle Shape and Internal Baffles. *Powder Technol.* **2015**, *286*, 732–739. [[CrossRef](#)]
20. He, S.Y.; Gan, J.Q.; Pinson, D.; Yu, A.B.; Zhou, Z.Y. Flow Regimes of Cohesionless Ellipsoidal Particles in a Rotating Drum. *Powder Technol.* **2019**, *354*, 174–187. [[CrossRef](#)]
21. Xie, C.; Song, T.; Zhao, Y. Discrete Element Modeling and Simulation of Non-Spherical Particles Using Polyhedrons and Super-Ellipsoids. *Powder Technol.* **2020**, *368*, 253–267. [[CrossRef](#)]
22. Ahmadian, H.; Hassanpour, A.; Ghadiri, M. Analysis of Granule Breakage in a Rotary Mixing Drum: Experimental Study and Distinct Element Analysis. *Powder Technol.* **2011**, *210*, 175–180. [[CrossRef](#)]
23. Cleary, P.W. DEM Prediction of Industrial and Geophysical Particle Flows. *Particuology* **2010**, *8*, 106–118. [[CrossRef](#)]
24. Colin, B.; Dirion, J.L.; Arlabosse, P.; Salvador, S. Wood Chips Flow in a Rotary Kiln: Experiments and Modeling. *Chem. Eng. Res. Des.* **2015**, *98*, 179–187. [[CrossRef](#)]
25. Gao, Y.; Muzzio, F.J.; Ierapetritou, M.G. A Review of the Residence Time Distribution (RTD) Applications in Solid Unit Operations. *Powder Technol.* **2012**, *228*, 416–423. [[CrossRef](#)]
26. Norouzi, H.R.; Zarghami, R.; Sotudeh-Gharebagh, R.; Mostoufi, N. *Coupled CFD-DEM Modeling: Formulation, Implementation and Application to Multiphase Flows*; John Wiley & Sons: Hoboken, NJ, USA, 2016; ISBN 1119005132.
27. Fu, P.; Bai, X.; Yi, W.; Li, Z.; Li, Y. Fast Pyrolysis of Wheat Straw in a Dual Concentric Rotary Cylinder Reactor with Ceramic Balls as Recirculated Heat Carrier. *Energy Convers. Manag.* **2018**, *171*, 855–862. [[CrossRef](#)]
28. Fogler, H.S. *Elements of Chemical Reaction Engineering*, 5th ed.; Prentice Hall: Upper Saddle River, NJ, USA, 2016.
29. Bérard, A.; Blais, B.; Patience, G.S. Experimental Methods in Chemical Engineering: Residence Time Distribution—RTD. *Can. J. Chem. Eng.* **2020**, *98*, 848–867. [[CrossRef](#)]
30. Cangialosi, F.; Di Canio, F.; Intini, G.; Notarnicola, M.; Liberti, L.; Belz, G.; Caramusco, P. Experimental and Theoretical Investigation on Unburned Coal Char Burnout in a Pilot-Scale Rotary Kiln. *Fuel* **2006**, *85*, 2294–2300. [[CrossRef](#)]
31. Chen, I.Y.; Navodia, S.; Yohannes, B.; Nordeck, L.; Machado, B.; Ardalani, E.; Borghard, W.G.; Glasser, B.J.; Cuitiño, A.M. Flow of a Moderately Cohesive FCC Catalyst in Two Pilot-Scale Rotary Calciners: Residence Time Distribution and Bed Depth Measurements with and without Dams. *Chem. Eng. Sci.* **2021**, *230*, 116211. [[CrossRef](#)]
32. Sai, P.S.T. Drying of Solids in a Rotary Dryer. *Dry. Technol.* **2013**, *31*, 213–223. [[CrossRef](#)]
33. Bongo Njeng, A.S.; Vitu, S.; Clause, M.; Dirion, J.L.; Debacq, M. Effect of Lifter Shape and Operating Parameters on the Flow of Materials in a Pilot Rotary Kiln: Part III. Up-Scaling Considerations and Segregation Analysis. *Powder Technol.* **2016**, *297*, 415–428. [[CrossRef](#)]
34. Sai, P.S.T.; Surender, G.D.; Damodaran, A.D.; Suresh, V.; Philip, Z.G.; Sankaran, K. Residence Time Distribution and Material Flow Studies in a Rotary Kiln. *Metall. Trans. B* **1990**, *21*, 1005–1011. [[CrossRef](#)]
35. Chatterjee, A.; Sathe, A.V.; Mukhopadhyay, P.K. Flow of Materials in Rotary Kilns Used for Sponge Iron Manufacture: Part II. Effect of Kiln Geometry. *Metall. Trans. B* **1983**, *14*, 383–392. [[CrossRef](#)]
36. Sudah, O.S.; Chester, A.W.; Kowalski, J.A.; Beeckman, J.W.; Muzzio, F.J. Quantitative Characterization of Mixing Processes in Rotary Calciners. *Powder Technol.* **2002**, *126*, 166–173. [[CrossRef](#)]
37. Sherritt, R.G.; Chaouki, J.; Mehrotra, A.K.; Behie, L.A. Axial Dispersion in the Three-Dimensional Mixing of Particles in a Rotating Drum Reactor. *Chem. Eng. Sci.* **2003**, *58*, 401–415. [[CrossRef](#)]
38. Third, J.R.; Scott, D.; Scott, S.A. Axial Dispersion of Granular Material in Horizontal Rotating Cylinders. *Powder Technol.* **2010**, *203*, 510–517. [[CrossRef](#)]
39. Gu, C.; Li, P.; Yuan, Z.; Yan, Y.; Luo, D.; Li, B.; Lu, D. A New Corrected Formula to Predict Mean Residence Time of Flexible Filamentous Particles in Rotary Dryers. *Powder Technol.* **2016**, *303*, 168–175. [[CrossRef](#)]
40. Liu, X.Y.; Specht, E. Mean Residence Time and Hold-up of Solids in Rotary Kilns. *Chem. Eng. Sci.* **2006**, *61*, 5176–5181. [[CrossRef](#)]
41. Hatzilyberis, K.S.; Androutopoulos, G.P. An RTD Study for the Flow of Lignite Particles through a Pilot Rotary Dryer Part i; Bare Drum Case. *Dry. Technol.* **1999**, *17*, 745–757. [[CrossRef](#)]
42. Bensmann, S.; Subagyo, A.; Walzel, P. Residence Time Distribution of Segregating Sand Particles in a Rotary Drum. *Part. Sci. Technol.* **2010**, *28*, 319–331. [[CrossRef](#)]
43. Nafsun, A.I.; Herz, F.; Liu, X. Influence of Material Thermal Properties and Dispersity on Thermal Bed Mixing in Rotary Drums. *Powder Technol.* **2018**, *331*, 121–128. [[CrossRef](#)]